HHS Public Access

Author manuscript

J Comp Neurol. Author manuscript; available in PMC 2018 July 07.

Published in final edited form as:

J Comp Neurol. 2017 December 01; 525(17): 3636–3652. doi:10.1002/cne.24292.

CLUSTERED ORGANIZATION AND REGION-SPECIFIC IDENTITIES OF ESTROGEN-PRODUCING NEURONS IN THE FOREBRAIN OF ZEBRA FINCHES (*Taeniopygia guttata*)

Maaya Z. Ikeda[^,1,3], **Amanda A. Krentzel**[^,2,3], **Tessa S. Oliver**[3], **Garrett B. Scarpa**[3], and **Luke Remage-Healey**[1,2,3,*]

[1]Molecular and Cellular Biology Program, University of Massachusetts, Amherst, MA 01003, USA

[2]Neuroscience and Behavior Program, University of Massachusetts, Amherst, MA 01003, USA

[3]Department of Psychological and Brain Sciences, University of Massachusetts, Amherst, MA 01003, USA

Abstract

A fast, neuromodulatory role for estrogen signaling has been reported in many regions of the vertebrate brain. Regional differences in the cellular distribution of aromatase (estrogen synthase) in several species suggest that mechanisms for neuroestrogen signaling differ between and within brain regions. A more comprehensive understanding of neuroestrogen signaling depends on characterizing the cellular identities of neurons that express aromatase. Calcium-binding proteins such as parvalbumin and calbindin are molecular markers for interneuron subtypes, and are co-expressed with aromatase in human temporal cortex. Songbirds like the zebra finch have become important models to understand the brain synthesis of steroids like estrogens and the implications for neurobiology and behavior. Here, we investigated the regional differences in cytoarchitecture and cellular identities of aromatase-expressing neurons in the auditory and sensorimotor forebrain of zebra finches. Aromatase was co-expressed with parvalbumin in the caudomedial nidopallium (NCM) and HVC shelf (proper name) but not in the caudolateral nidopallium (NCL) or hippocampus. By contrast, calbindin was not co-expressed with aromatase in any region investigated. Notably, aromatase-expressing neurons were found in dense somato-somatic clusters, suggesting a coordinated release of local neuroestrogens from clustered neurons. Aromatase clusters were also more abundant and tightly packed in the NCM of males as compared to females. Overall, this study provides new insights into neuroestrogen regulation at the network level, and extend previous findings from human cortex by identifying a subset of aromatase neurons as putative inhibitory interneurons.

Keywords

Aromatase; estradiol; parvalbumin; calbindin; auditory; microcircuit; pallium; RRID: AB_476894; RRID: AB_2174013; RRID: AB_2092365; RRID: AB_2298772

[*]Corresponding author: Luke Remage-Healey.

[^]M.Z.I. and A.A.K. contributed equally to this study.

Conflict of interest statement. There are no identified conflicts.

Introduction

Songbirds, especially zebra finches, are one of the most useful models to study rapid estrogen signaling in the brain (Saldanha et al., 2011)(Remage-Healey, 2014). Research in songbirds has led to advances in understanding the neurobiological mechanisms underlying the perception and production of complex sounds (Mooney, 2009; Maney, 2013; Comins and Gentner, 2014). Interestingly, the neural circuits for auditory and spatial processing in songbirds express abundant levels of aromatase, the enzyme required for estradiol synthesis (Saldanha et al., 2000; Remage-Healey et al., 2008). Similarly, in humans, aromatase positive neurons are found in nearly all layers of temporal cortex (Yague et al., 2006). In zebra finches, high expression of aromatase is found in the caudomedial nidopallium (NCM), a region analogous to the mammalian secondary auditory cortex (Shen et al., 1995; Saldanha et al., 2000; Peterson et al., 2005) and other regions involved in auditory processing and song control are found to express aromatase to different degrees (Vockel et al., 1990; Jacobs et al., 1999; Saldanha et al., 2000). Although many studies at the molecular, cellular, and physiological levels have elucidated key aspects of estrogen signaling in the avian brain (Baillien and Balthazart, 1997; Balthazart et al., 2001, 2003, 2005, 2006, 2011, Remage-Healey et al., 2008, 2009, 2010, 2011; Jeong et al., 2011; Remage-Healey and Joshi, 2012; Charlier et al., 2013, 2016; Comito et al., 2016), the connectivity, organization, and identity of aromatase neurons are not well understood.

Characterizing the distribution and cellular identity of aromatase-positive neurons is necessary to fully understand neuroestrogen signaling. In the mammalian cortex, interneurons have been classified based on morphology, connectivity, physiological properties, and neuronal markers such as calcium binding proteins (reviewed by Markram et al., 2004). Although our knowledge about the function of calcium binding proteins and their significance in neuronal network patterning is incomplete, these markers provide a reliable way of categorizing and measuring the heterogeneity of cortical neurons. Parvalbumin (PV) and calbindin (CB) are conventional interneuron markers (Kawaguchi and Kubota, 1997a; Markram et al., 2004). Although there are some exceptions, in many mammalian brain regions, PV and CB are expressed in inhibitory interneurons, and are associated with distinct activity patterns (Kawaguchi and Kubota, 1997b; Markram et al., 2004; Runyan et al., 2010). In the temporal cortex of humans and monkeys, aromatase is co-expressed with both PV and CB in neurons (Yague et al., 2006, 2008). In the songbird NCM, neurons with different spiking kinetics, including GABAergic interneurons, are specialized for certain aspects of auditory processing (Pinaud and Mello, 2007; Schneider and Woolley, 2013; Asik and Kirn, 2015; Ono et al., 2016; Yanagihara and Yazaki-Sugiyama, 2016) and GABAergic neurons are active when birds hear songs (Pinaud and Mello, 2007). Together, these observations raise the possibility that auditory-evoked changes in the activity of GABAergic neurons are directly linked to auditory-evoked elevations in forebrain estradiol levels (Remage-Healey et al., 20082008).

In this study, we tested the hypothesis that the cytoarchitecture and cellular identity of aromatase positive cells in the zebra finch NCM are similar to that in the temporal cortex of primates. In a broad survey of brain areas, we examined the cellular distribution of aromatase-positive neurons and tested whether they co-express PV or CB. Our results show

that some aromatase positive neurons are positive for PV but, unlike in the primate temporal cortex, none are positive for CB, suggesting a species difference in the mechanism of estradiol signaling at the circuit level. Interestingly, the co-expression of PV and aromatase in neurons is also region specific, as it is found only in NCM and a region surrounding sensorimotor HVC. In addition, examination of aromatase expressing neurons at high resolution revealed unexpected clustering of cell bodies of estrogen-producing neurons in many regions of the songbird brain, which could be important for cell-to-cell interactions and an unusually high cell packing density (Olkowicz et al., 2016).

Materials and Methods

Animals

Adult (> 110 days post-hatch) male (N=7) and female (N=6) zebra finches were selected from single sexed cages in a mixed sex aviary room (i.e., all birds in this study were not actively breeding) with food and water available *ad libidum*. Most of these birds (N=12) were isolated in sound attenuating chambers overnight maintained on a 14L:10D light cycle. Between 10:00am–12:00pm the following day birds were exposed to conspecific songs for 30 min. After the playbacks, the birds were housed in the dark for 30 min. These procedures were performed because tissues from a subset of the animals were used for a separate pilot study involving visualization of song-induced immediate early gene expression. The conditions were kept the same for the rest of the animals to control for potential variability in aromatase expression caused by the playbacks. One additional animal (male) did not go through the playback procedure but this tissue was not used for quantifications and only used to determine the staining pattern of NeuN and PSD-95. The pattern of aromatase staining in sections from this animal was indistinguishable from the staining of tissue from animals exposed to playbacks.

The birds were euthanized by isoflurane overdose, transcardially perfused with 0.1M phosphate buffer with 0.9% saline (PBS) followed by 4% paraformaldehyde. The brains were extracted, post-fixed in 4% paraformaldehyde at room temperature for 2hrs, and submerged in 30% sucrose PB in 4 °C overnight. The brains were then molded in OCT compound and sectioned sagittally at 35μm using a cryostat (Leica, Germany). The sections were kept in −20 °C in cryoprotectant (30% sucrose/30% ethylene glycol/1% polyvinylpyrrolidone) at 4 °C in phosphate buffer (PB) until use.

Immunocytochemistry

Brain sections were washed thoroughly with PB, permeabilized and blocked with 10% normal goat serum in 0.3% phosphate buffer Triton X (PBT) for 2hrs at room temperature, and incubated with primary antibodies diluted in 0.3% (PBT) (see Table 1 for dilutions) at room temperature for 1hr and then at 4 °C for two nights (<48hrs). Each antibody used here showed patterns of cellular morphology and distribution consistent with previous publications, as cited below in “Antibodies”. After the primary incubation, the sections were washed with 0.1% PBT three times for 15 min each and were incubated in secondary antibodies (anti-rabbit, anti-mouse, and/or anti-guinea pig; either Alexa 488-or Alex 594-conjugated, raised in goat, Thermo Fisher Scientific Inc., MA, USA; 1/200) for 1hr at room

temperature. The sections were washed three times for 15 min each in 0.1% PBT and once in PB. The sections were mounted onto gelatin-coated slides and coverslipped using ProLong Diamond Antifade Mounting Medium (Thermo Fisher).

Antibodies

All antibodies used are listed in Table 1.

1. The antibody against the zebra finch aromatase was a polyclonal antibody raised in rabbit. This antibody was generously provided by Dr. Colin Saldanha. The specificity of this antibody has been previously verified in zebra finch tissue using western blots and the negative binding in tissue pre-absorbed with the immunogen (Saldanha et al., 2000). Region-specific staining pattern with this antibody in the present study matches that previously reported (Saldanha et al., 2000). Immunoblots showing a single band have been more recently published for this same antibody, confirming its viability (Rohmann et al., 2007; Mehos et al., 2016)

2. Anti-calbindin antibody (Sigma Aldrich, C9848, RRID: AB_476894) was raised against bovine kidney calbindin-D (manufacturer's technical information). Previously, the specificity of this antibody has been determined by the presence of a single band western blot in quail and rodent brain tissue (Moe et al., 2016). Our staining pattern with the antibody in zebra finch tissue matches that of a previously reported distribution using a specific antibody raised against the chicken calbindin protein (Pinaud et al., 2006)

3. Anti-parvalbumin antibody (Millipore, MAB1572, RRID: AB_2174013) was raised against parvalbumin protein purified from frog muscle (manufacturer information). The specificity of the antibody has been shown using western blot (Li et al., 2013). Our staining pattern in the zebra finch is identical to previously reported distributions using a different specific antibody (Wild et al., 2005).

4. Anti-post-synaptic density protein 95 (PSD95) antibody (Millipore, MAB 1596, RRID: AB_2092365) was raised against recombinant rat PSD95 (manufacturer information). The specificity of this antibody has been determined by the presence of a single band western blot in chicken brain tissue (Chaudhury et al., 2010).

5. Anti-NeuN antibody (Millipore, MAB377, RRID: AB_2298772) was raised against purified cell nuclei from mouse brain (manufacturer information). This antibody is a specific neuronal marker and its cell-type specificity has been shown using western blot and analysis in brain sections of various species including chickens (Mullen et al., 1992). When brain sections are double-labeled with an anti-GFAP (Glial fibrillary acidic protein, glial marker) antibody, the signals do not overlap, indicating that anti-NeuN does not mark glial cells.

Confocal imaging

Fluorescently labeled sections were imaged using a confocal microscope (NA1, Nikon, Tokyo, Japan) with NIS-Elements imaging software (Ar; RRID: SCR_002776). The laser

strength and gain were determined separately for each section to adjust for the intensity of the staining across sections; however, the imaging settings were kept consistent across regions within each section (See Figure 3e–j for the regions of interest). Pictures of the NCM (ventral and dorsal), CMM, and HP were taken from sections 0.2–1mm lateral to the midline and pictures of HVC, HVC shelf, NCL, RA were taken from sections 1.7–2.5mm lateral to the midline. Since the boundaries between the NCL and NCM and between the arcopallium and NCL are not yet clearly defined for songbirds, the medial-most aspect of nucleus taeniea (Tn; rich aromatase expression) was used as a landmark for the lateral boundary of the NCM, and pictures of the NCL were taken from sections that were in-plane with RA. For each section, stitch images using 10× magnification were taken and used to observe the overall pattern of the staining in the sections and as a reference for higher magnification images (60×, oil; see Figure 3a–d). Once regions were identified, 60× images were taken using z-stack settings (1μm z-steps for 9–15μm). Zoomed-in images of individual neurons or clusters (Figure 9m–s were taken using smaller z-step sizes (0.1μm–0.5μm).

Image analysis

The number of immunostained cells and the total number of cells (DAPI-positive nuclei) in each unprocessed z-stack image were counted by blinded experimenters using FIJI software (National Institutes of Health, USA, RRID: SCR_002285). The images presented in the figures were adjusted for contrast and brightness for clarity. For each region, the numbers of aromatase-positive cells were divided by the number of DAPI+ stained nuclei to calculate the percentage of aromatase positive cells per total number of cells (percentage of aromatase + cells). Co-expression of two antigens was unambiguously confirmed by comparing both maximum intensity projection images and individual z-slice images for every image (z-slice images ranged from 9 μm to 15μm thickness). Some cells were negative for aromatase but were densely innervated by aromatase-positive terminals (“ghost cells”; as previously described in Saldanha et al., 2000). Examples of “ghost cells” and “aromatase-expressing” cells are shown in Figure 1a&b. Previously, Saldanha et al. (2000) showed that only terminal aromatase is found in the arcopallium while somatic aromatase cells are found in the NCL. In situ results for aromatase mRNA have also reported aromatase in the lateral aspect of the caudal nidopallium (Jacobs et al., 1999). In our sections, we found high intensity cells in the NCL and ghost cells in the nearby arcopallium within the same image. When sections were double-labeled with the post synaptic marker postsynaptic density protein 95 (PSD-95) and with aromatase, ghost cells showed higher signals for PSD-95 than aromatase-expressing cells (Figure 1b). When zoomed-in, many of the PSD-95 signals co-localized with aromatase signals (Figure 2c&f). This is consistent with the interpretation that ghost cells are likely to be neurons receiving aromatase+ afferents and not expressing intracellular aromatase protein. In HVC and arcopallium, although there are no aromatase+ somatas, the presence of pre-synaptic aromatase terminals (Saldanha et al., 2000; Peterson et al., 2005) and aromatase activity (Vockel et al., 1990; Rohmann et al., 2007) has been reported in these regions. We carried out a separate analysis measuring the optical density of randomly chosen cells (N=15 somatic and N=24 “ghost” cells from 11 pictures taken in 5 regions), confirming that cells that were classified in our analysis as aromatase+ cells had significantly higher optical density than “ghost” cells (unpaired T-test, $p < 0.0001$; OD: somatic 2.13+/− 0.24;

ghost 0.87 +/− 0.11). To avoid including potential neurons that were negative for aromatase but were densely innervated by aromatase-positive terminals, “ghost cells” were excluded from analysis for all cell counts in this study.

Clusters were defined as a group of two or more cells forming somato-somatic contacts (i.e. zero distance between the cell bodies at 60× magnification). The number of cells within each cluster was counted manually by scrolling through z-stack images in FIJI. We ran a simulation using MATLAB to determine whether clustering of aromatase somas is different from what can be expected by random association. We sampled from a normal distribution using the mean and SEM from the aromatase cell count (91.7±7.29) for the cluster analysis. We created random plots of spheres varying by cell number and size (also sampling from a normal distribution: average diameter of 50 somas measured was 9.16±0.29 μm). The plot was fit to the dimensions of our images, including the volume (15μm). We ran 1000 simulations and quantified the distance between all the spheres per simulation. Points were defined as making sphere-sphere contacts or “a cluster” when their distance was shorter than the sum of each sphere’s radius. After 1000 simulations, a percentage of spheres found in cluster sizes of 1, 2, 3… etc. were quantified using the union-find algorithm. This simulation quantification mirrors that of the manual aromatase cell clustering counts performed on our images.

Data analysis

Statistical analyses were performed using the statistical software packages R and Origin 2017. One-way ANOVA (ANOVA), two-way ANOVA (TW-ANOVA), or post hoc *t*-tests were conducted when appropriate. For aromatase clusters, we conducted a two-way mixed effects ANOVA for sex and cluster size comparisons. Post hoc comparisons were conducted with Bonferroni corrections. For comparisons to the simulation percentages, since we used 1000 simulations to generate random values we generated a population mean and then conducted one-sample t-test for each cluster size and each sex against this population mean.

Results

The neuronal composition of aromatase positive nuclei is region-dependent

To examine the identities of estrogen-producing cells, zebra finch brains were immunostained with antibodies against the zebra finch aromatase (Figure 3k–r), and co-labeled with other neuronal markers (Figure 4a–l). In agreement with previous findings, the percentages of aromatase+ cells were high in the NCM and HVC shelf (Saldanha et al., 2000) and no aromatase+ cells were found in the ventral CMM (Figure 3). No difference in the percentages of aromatase+ cells was found between ventral and dorsal NCM. The percentage of aromatase+ cells was significantly higher in the hippocampus (HP) than in other regions (Figure 3s ; ANOVA for all regions: $F(7, 67) = 7.46$, $p< 0.0001$; post-hoc t-tests: HP vs any region, $p < 0.05$; CMM vs any region, $p<0.01$; CMM, N= 10; NCMv, N= 11; NCMd, N= 11; HP, N= 11; NCL, N= 8; HVC shelf A, N= 8; HVC shelf V, N= 8; HVC shelf P, N= 8). Notably, the total number of aromatase-positive cells in the NCL were comparable to that of the NCM (Figure 3s), suggesting the importance of estrogen synthesis in both of these regions. There were no sex differences in the total number of aromatase-

positive cells (TW-ANOVA main effect sex: F(1,62)=1.72, p=0.19) including NCM (Figure 3t), which is consistent with previous reports (Saldanha et al. 2000). Individual comparisons between males and females for aromatase density broken down by brain regions are the subject of a separate study (Krentzel, Ikeda, Koroveshi, and Remage-Healey, unpublished observations).

Double-labeling immunocytochemistry of aromatase+ cells with antibodies against NeuN showed that > 99% of aromatase cells were neurons (for example, see Figures 6&7). This is in agreement with a previous study showing that most aromatase+ cells in the uninjured zebra finch brain are non-glial (Peterson et al., 2004). Furthermore, double-staining for aromatase-ir and calbindin-ir showed that none of the aromatase positive neurons express calbindin in any regions investigated (Figure 4g–l). By contrast, some aromatase+ neurons were positive for parvalbumin (Figure 4a–f). The mean percentage of PV+ aromatase+ neurons was different within and among regions (Figure 5); ANOVA: region, $p<0.0001$. Post-hoc Tukey tests significant comparisons ($p<0.05$): NCMv vs. all regions and HVCshelfp vs. HVCshelfa.. Parvalbumin-expressing aromatase cells were mostly found in the NCM and the HVC shelf. Within the NCM, a higher percentage of aromatase+ neurons co-expressed with parvalbumin was found in the ventral region (15%) than the dorsal region (5%). Importantly, the amount of co-expression between PV and aromatase was highly variable across subjects and, in the dorsal NCM of some subjects, the overlap between PV and aromatase was 0. The individual variability for PV was not due to the location where images were taken and could also not be explained by sex (TW-ANOVA: sex, $F(1, 47)= 0.75$, $p= 0.39$; region, $F(7, 47)= 7.3$, $p< 0.001$; sex*region, $F(7,47)= 0.14$, $p= 0.99$. CMM, N= 9 (F, N=5; M, N=4); NCM, N=10; HP, N= 9 (F, N=6; M, N=3): NCL, N= 5 (F, N=3; M, N=2): HVC shelf A, N= 7 (F, N=2; M, N=5); HVC shelf V, N= 6 (F, N=3; M, N=3); HVC shelf P, N= 7). Although the percentage of aromatase+ cells was high in the HP and NCL, only a few of these cells (<1%) co-expressed parvalbumin (Figure 5). Therefore, NCM aromatase+ neurons are a mixture of a small number of parvalbumin+ neurons and many of other types of neurons (>85%) whose identity is unknown. Further, the contrast in the proportion of parvalbumin-positive, aromatase+ cells between the NCM and NCL supports the idea that the control and context for estrogen synthesis are different between these regions, despite the common presence of high levels of aromatase in each region (this study; Jacobs et al., 1999; Saldanha et al., 2000). Overall, the density and identity of aromatase+ cells in the songbird forebrain appears to be highly region-specific.

Aromatase-expressing neurons form clusters with other neurons in NCM

The microcircuit organization of estrogen-producing neurons can provide clues about the control of neuroestrogen synthesis and action. A striking characteristic of the aromatase+ neurons we observed in NCM is that they form somatic clusters with other neurons (Figure 6a–f). Clear somatic clusters were found in all regions except in the HP (Figure 6g–l). In the HP, neurons were found to be in contact with other neurons, but those aggregations were less compact and discrete than clusters in other regions we analyzed (see also Fig. 7a–f). Detailed analysis of a double-label staining for aromatase and NeuN in the ventral NCM revealed that NCMv neurons are predominantly found in clusters (78.2%) and that the majority of neurons were positive for aromatase (65.2%, Figure 8a). Analyses of pictures

from all animals showed that the majority of aromatase+ neurons are in contact with at least one other aromatase+ neuron (65.2± 5.76 %) and many are found in large clusters composed of more than three neurons (Figure 8b&c). Both parvalbumin+ and calbindin+ cells were found in clusters with aromatase+ cells (Figure 9&10), suggesting that local estrogen signaling likely impacts inhibitory microcircuits within NCM.

We observed a sex by cluster size interaction in the occurrence of aromatase clusters in ventral NCM ($F(8,72)=3.10$, $p=.0046$; Figure 8c). More aromatase cells in females (47.4%) are not clustered as opposed to in males (26.4%; Bonferroni pairwise comparison $t(72)=5.27$, $p<.001$, Figure 8c). Most aromatase cells are clustered with at least another aromatase cell (females 52.6%, males 73.6%). We then wanted to determine the extent to which these clustered distributions would be observed by chance, and we ran simulations to determine how often similar cell-sized spheres would cluster together in a simple computational model. We found that both males ($t(4)=-10.89$,$p<.001$) and females ($t(5)=-3.04$,$p=.029$) have a lower proportion of cells not clustered than random (males=26.4%, females=47.4%, random=72.8%; Figure 8b), as well as a higher proportion of clustered cells (males: $t(4)=11.05$, $p<.001$, females: $t(5)=3.13$, $p=.026$, random 26.5%). Males had more frequent occurrences of large cell clusters as well as more subjects that had cases of large clusters, which was rare in our simulation and did not occur as often in females (summary of sex differences in Table 2). We detected a significant main effect of cluster size ($F(8,72)=31.39$, $p<0.00001$). The decline in the percent of aromatase cells found in increasing cluster sizes differed between the sexes. For males, aromatase cells found solo (1), with another aromatase cell (2), and in a cluster of 3 or 4 did not significantly differ from each other (pairwise Bonferroni comparisons: 1vs.2 $t(72)=0.44$, $p>.05$, 1vs.3 $t(72)=0.59$, $p>.05$, 1vs.4 $t(72)=3.72$, $p=0.06$; Figure 8c). However, cluster sizes of 5 and above were significantly different than non-clustered aromatase cells (1vs≥5, $p<.05$), but not significantly different from each other (Figure 8c). By contrast, in females non-clustered aromatase cells were significantly different than all cluster sizes (pairwise Bonferroni comparisons: 1vs.2 $t(72)=3.81$, $p<.0001$, etc., Figure 8c) and continued to decline. We considered the reason that males may have more clustering than females if they have a greater cell density within this region. However, we compared DAPI measurements from ventral NCM and found no differences between either sex in NCMv ($t(9)=-0.72$, $p=0.49$; data not shown).

Aromatase+ cells without NeuN expression are found along the ventricles

Regardless of the region, remote occurrences of isolated aromatase+ cells were found at the edges of the tissue including regions with low numbers of aromatase+ neurons, such as HVC, CMM, and ventral HP (Figures 11 & 12). Although HVC was mostly negative for somatic aromatase+ cells, isolated cells with high-intensity aromatase-ir were occasionally found within the bounds of HVC (Figure 11d–f). Similarly, sparse and isolated aromatase+ cells were found in the dorsal CMM close to the ventricle (Metzdorf et al., 1999, Figure 11). In most cases, these sporadic aromatase+ cells co-expressed NeuN when their cell bodies were at distance (i.e., > 0μm) from the ventricle, whereas aromatase+ cells with cell bodies in contact with the edge of the tissue were negative for NeuN (Figures 11c–i). We did not observe large morphological differences in aromatase+ cells that were positive vs. negative

for NeuN (i.e., compare the morphology of aromatase+ cells indicated by arrows (NeuN-) vs arrowheads (NeuN+) in Fig. 11c–e).

Discussion

The current study examined the regional differences in distribution, organization, and identities of aromatase expression in the zebra finch forebrain. The anatomical observations described here provide evidence for regional heterogeneity in the neurochemical identity and cytoarchitecture of aromatase neurons. First, we report that although many brain regions express aromatase, the identities of the neurons expressing aromatase differ substantially between regions. Specifically, the interneuron marker parvalbumin was expressed in a portion of aromatase+ neurons in the NCM. By contrast, in the HP and NCL, where the percentage of aromatase positive neurons were equivalent to or greater than that of the NCM, parvalbumin was not co-expressed with aromatase. This study is, to our knowledge, the first to provide direct anatomical evidence for the differences in neuronal makeup between the NCL and NCM, and to report that the amount of aromatase expressed in NCL is equivalent to that of the NCM (see also qualitative descriptions in Jacobs et al., 1999). Moreover, the observations that aromatase+ neurons in the NCM were a mixture of parvalbumin positive and negative neurons and that the percentage of co-expression was different between ventral and dorsal NCM suggest that local neuroestrogen synthesis is differentially regulated within and between subregions of the NCM itself. Since aromatase activity can be driven by neuronal activity (Balthazart et al., 2001, 2006; Remage-Healey et al., 2009), our study suggests that estrogen synthesis could be under exceedingly localized control in different classes of neurons within and between brain regions. Indeed, in the zebra finch brain, there are variations in control of aromatase activity dependent on brain region (Comito et al. 2016). In addition, the fact that aromatase+ cells in the human temporal cortex consists of glia and neurons, some of which expresses calbindin or parvalbumin, should be taken into account when comparing human and avian co-localization patterns (Yague et al., 2006, 2008). The connection between estrogen synthesis and PV neurons in particular is intriguing in our study, given that PV neurons are key for sensory plasticity during early developmental critical periods (Hensch, 2005; He et al., 2014; Werker and Hensch, 2015). The neuroplasticity enabled by the actions of estrogens in a variety of brain regions and species (e.g., Barha and Galea, 2010; Zimmerman et al., 2011; Frick, 2012; Banerjee and Liu, 2013; Srivastava et al., 2013) may therefore be due to the synthesis of, and actions upon, estrogens in PV-expressing interneurons.

In the HP, we found more aromatase+ somatas than in any other regions we analyzed, while in a previous study, there were fewer cell bodies expressing aromatase in the HP compared to the NCM (Saldanha et al., 2000). If this discrepancy is not methodological in origin, it may be due to a difference in hormonal conditions of the animals, since HP aromatase levels are sensitive to circulating estradiol levels (Saldanha et al., 2000).

Second, we observed that neurons are found in discrete somato-somatic clusters in the NCM, and that aromatase-expressing neurons are likewise densely packed into clusters. In songbirds, cell clusters in the brain have been previously described in a handful of studies (Fortune and Margoliash, 1992; Fortune et al., 1995; Gahr and Garcia-Segura, 1996; Kirn et

al., 1999; Medina et al., 2013). In zebra finches, cell clusters have been reported in the nidopallium, mesopallium, and hyperpallium (Fortune and Margoliash, 1992; Fortune et al., 1995; Medina et al., 2013). Medina et al. (2013), suggested that the clusters in the mesopallium are composed of one neuron and multiple glial cells, based on Nissl stain. Our use of NeuN staining here indicates that the majority of the clusters are composed of neurons in all regions we examined, including the NCM and CMM (i.e., in both nidopallium and mesopallium). In the ventral NCM, many aromatase+ neurons were found in clusters, which suggests a role for coordinated communication in the regulation of aromatase activity. Little is known about the physiology of neuronal clusters in songbirds, with the exception of one study showing that neuronal clusters in canary HVC are coupled via gap junctions (Gahr and Garcia-Segura, 1996). Dye transfer between aromatase-expressing cells and adjacent cells has also been reported in the quail hypothalamus (Cornil et al., 2004), suggesting a mechanism for the control of neuroestrogen synthesis within clusters of aromatase-positive neurons. More broadly, electrical coupling is a feature of neuroendocrine secretion patterns in many species. Neuronal synchronization is dependent on functional gap junctions for the pulsatile release of GnRH in the hypothalamus (Pinet-Charvet et al., 2016), for reproductive neurohormone release in aplysia (Dargaei et al., 2014), and for coordinated neurosecretion in the supraoptic nucleus (Yang and Hatton, 1988) and suprachiasmatic nucleus (Colwell, 2000; Long et al., 2005).

In mammalian cortex, the majority of gap junctions are observed between two inhibitory neurons or between inhibitory and excitatory neurons (Connors et al., 1999; Hestrin and Galarreta, 1999; Venance et al., 2000; Meyer et al., 2002), and parvalbumin-expressing or fast-spiking neurons are known to be connected via gap junctions (Hestrin and Galarreta, 1999; Meyer et al., 2002; Fukuda and Kosaka, 2003). In this present study, we found that both parvalbumin- and calbindin-positive neurons occur within clusters, raising the possibility of communication via somato-somatic gap junctions. In this context, we also found a notable sex difference in that males had greater occurrences of aromatase somato-somatic clusters than did females. Depending on the physiological nature of clusters, this suggests an intimate, coordinated communication among aromatase cells in the NCM of males.

These observations now open new directions regarding the physiological interaction among aromatase neurons and the implications for auditory processing and neuroestrogen modulation. Regardless of whether clustered aromatase neurons in forebrain regions like the songbird NCM are electrically coupled, their close apposition indicates a high likelihood of coordinated neuroestrogen synthesis and release. Cellular clusters also may be one of the ways songbirds achieve the high packing density of neurons in the forebrain, which is exceptionally elevated compared to mammals (Olkowicz et al., 2016). The sex differences we observed in aromatase clustering patterns indicates sex specificity in aromatase regulation at the level of neuronal and neural circuit function.

Third, we occasionally found sporadic, isolated neurons with intense aromatase signals in the HVC, CMM, and in areas close to the edge of the telencephalon. In canaries, aromatase mRNA has been reported along the lateral ventricle (Metzdorf et al., 1999). In neural injury experiments with zebra finches, a previous report showed that ventricular aromatase+ cells

were morphologically similar to radial glia marker-expressing cells as well as the expression pattern (Peterson et al., 2004). We found that although many aromatase+ cells that were at the lateral edge of the tissue were negative for NeuN, nearby aromatase+ cells that were further from the edge of the tissue were positive for NeuN. In the CNS, neurons and radial glia are born in the ventricular zone, and radial glia give rise to migrating neurons (Alvarez-Buylla et al., 1990; Noctor et al., 2001). Resultant hypotheses from the current observations are that the aromatase+ cells at the edge of the tissue are radial glia (such as has been observed in teleosts (Forlano et al., 2006)) and/or migrating newborn cells destined to become neurons themselves. Some newborn cells in the ventricular zone lack NeuN expression, as well as some mature neurons (Mullen et al, 1992). Although the functions and the identities of these cells along the ventricle border were not pursued in the current study, the differentiation and potential incorporation of these cells into circuits like HVC should be examined in future studies.

Lastly, we observed that calbindin and aromatase represent two non-overlapping cell types in the songbird forebrain. Previous reports in NCM have hypothesized that aromatase cells are colocalized with calbindin cells based on overlapping regional expression (Pinaud et al. 2005). However, this is the first time that aromatase and calbindin have been directly compared in the same neurons in the songbird brain, and we can now exclude the possibility that aromatase neurons in these regions are calbindin-positive interneurons, unlike in the human cortex (Yague et al. 2006). Calbindin and parvalbumin aromatase-negative neurons form clusters with aromatase-positive neurons, suggesting a role for these neuronal subtypes in neuroestrogen regulation and paracrine signaling, despite their lack of cellular co-localization.

In conclusion, the current study provides compelling anatomical evidence for regional differences in neuroestrogen regulation in the songbird brain. Our findings demonstrate that future work in this topic must take into account regional differences, neuronal circuits within and across regions, cell types, and cellular organization when studying neuroestrogen regulation. Further studies will need to characterize the substantial heterogeneity and clustering of aromatase neurons in the forebrain. By understanding the cellular identities of estrogen-producing neurons, targeted approaches can be developed to determine how estrogen signaling plays a role in sensory processing and cognitive function.

Acknowledgments

This research was supported in part by the NIH (R01NS082179), the NSF (IOS1354906), and the University of Massachusetts

Role of Authors. All authors had full access to all the data in the study and take responsibility for the integrity of the data and the accuracy of the data analysis. Study concept and design: M.Z.I., A.A.K., and L.R.H. Acquisition of data: M.Z.I., A.A.K., T.S.O. and G.B.S. Analysis and interpretation of data: M.Z.I., A.A.K., and L.R.H. Drafting of the manuscript: M.Z.I. Critical revision of the manuscript for important intellectual content: M.Z.I., A.A.K., and L.R.H.. Statistical analysis: M.Z.I., A.A.K. Obtained funding: L.R.H. Administrative, technical, and material support: L.R.H. Study supervision: L.R.H..

Other ACKNOWLEDGEMENTS

We thank Colin Saldanha (American University) for generously providing the anti-aromatase zebra finch antibody and Dr. Jim Chambers for assistance in confocal imaging.

Literature Cited

Alvarez-Buylla A, Theelen M, Nottebohm F. Proliferation “hot spots” in adult avian ventricular zone reveal radial cell division. Neuron. 1990; 5:101–109. [PubMed: 2369518]

Asik K, Kirn JR. Incorporation of parvalbumin expressing neurons in the caudomedial nidopallium (NCM) of juvenile zebra finches is affected by song tutor availability. Neurosci Meet Planner Washington, DC Soc Neurosci:Program#/Poster#: 289.02/A2. 2015

Baillien M, Balthazart J. A Direct Dopaminergic Control of Aromatase Activity in the Quail Preoptic Area. 1997; 63:99–113.

Balthazart J, Baillien M, Ball GF. Rapid and Reversible Inhibition of Brain Aromatase Activity. 2001; 13

Balthazart J, Baillien M, Ball GF. Rapid control of brain aromatase activity by glutamatergic inputs. Endocrinology. 2006; 147:359–66. [PubMed: 16195408]

Balthazart, J., Baillien, M., Ball, GF. Rapid Control of Brain Aromatase Activity by Glutamatergic Inputs. 2011. http://dx.doi.org/101210/en2005-0845

Balthazart J, Baillien M, Charlier TD. Calcium-dependent phosphorylation processes control brain aromatase in quail. 2003; 17:1591–1606.

Balthazart J, Baillien M, Charlier TD, Ball GF. Effects of Calmodulin on Aromatase Activity in the Preoptic Area. J Neuroendocrinol. 2005; 17:664–671. [PubMed: 16159379]

Banerjee SB, Liu RC. Storing maternal memories: hypothesizing an interaction of experience and estrogen on sensory cortical plasticity to learn infant cues. Front Neuroendocrinol. 2013; 34:300–14. [PubMed: 23916405]

Barha CK, Galea LAM. Influence of different estrogens on neuroplasticity and cognition in the hippocampus. Biochim Biophys Acta - Gen Subj. 2010; 1800:1056–1067.

Charlier TD, Cornil CA, Balthazart J. Rapid modulation of aromatase activity in the vertebrate brain. J Exp Neurosci. 2013; 7:31–7. [PubMed: 25157205]

Charlier TD, Harada N, Balthazart J, Cornil CA. Human and Quail Aromatase Activity Is Rapidly and Reversibly Inhibited by Phosphorylating Conditions. 2016; 152:4199–4210.

Chaudhury S, Jain S, Wadhwa S. Expression of synaptic proteins in the hippocampus and spatial learning in chicks following prenatal auditory stimulation. Dev Neurosci. 2010; 32:114–24. [PubMed: 20453464]

Colwell CS. Rhythmic coupling among cells in the suprachiasmatic nucleus. J Neurobiol. 2000; 43:379–88. [PubMed: 10861563]

Comins JA, Gentner TQ. Auditory temporal pattern learning by songbirds using maximal stimulus diversity and minimal repetition. Anim Cogn. 2014; 17:1023–1030. [PubMed: 24526277]

Comito D, Pradhan DS, Karleen BJ, Schlinger BA. Region-specific rapid regulation of aromatase activity in zebra finch brain. J Neurochem. 2016; 136:1177–1185. [PubMed: 26709964]

Connors BW, Gibson JR, Beierlein M. Two networks of electrically coupled inhibitory neurons in neocortex. Nature. 1999; 402:75–79. [PubMed: 10573419]

Cornil CA, Seutin V, Motte P, Balthazart J. Electrophysiological and neurochemical characterization of neurons of the medial preoptic area in Japanese quail (Coturnix japonica). Brain Res. 2004; 1029:224–240. [PubMed: 15542078]

Dargaei Z, Colmers PLW, Hodgson HM, Magoski NS. Electrical coupling between Aplysia bag cell neurons: characterization and role in synchronous firing. J Neurophysiol. 2014; 112

Fortune ES, Margoliash D. Cytoarchitectonic organization and morphology of cells of the field L complex in male zebra finches (Taenopygia guttata). J Comp Neurol. 1992; 325:388–404. [PubMed: 1447407]

Fortune ES, Margoliash D, Fortune. Parallel pathways and convergence onto HVc and adjacent neostriatum of adult zebra finches (Taeniopygia guttata). J Comp Neurol. 1995; 360:413–41. [PubMed: 8543649]

Frick KM. Building a better hormone therapy? How understanding the rapid effects of sex steroid hormones could lead to new therapeutics for age-related memory decline. Behav Neurosci. 2012; 126:29–53. [PubMed: 22289043]

Fukuda T, Kosaka T. Ultrastructural study of gap junctions between dendrites of parvalbumin-containing GABAergic neurons in various neocortical areas of the adult rat. Neuroscience. 2003; 120:5–20. [PubMed: 12849736]

Gahr M, Garcia-Segura LM. Testosterone-dependent increase of gap-junctions in HVC neurons of adult female canaries. Brain Res. 1996; 712:69–73. [PubMed: 8705309]

He L, Liu N, Cheng T, Chen X, Li Y, Shu Y, Qiu Z, Zhang X. Conditional deletion of Mecp2 in parvalbumin-expressing GABAergic cells results in the absence of critical period plasticity. Nat Commun. 2014; 5:5036. [PubMed: 25297674]

Hensch TK. Critical Period Mechanisms in Developing Visual Cortex. Current topics in developmental biology. 2005; 69:215–237. [PubMed: 16243601]

Hestrin S, Galarreta M. A network of fast-spiking cells in the neocortex connected by electrical synapses. Nature. 1999; 402:72–75. [PubMed: 10573418]

Jacobs EC, Arnold AP, Campagnoni AT. Developmental regulation of the distribution of aromatase- and estrogen-receptor- mRNA-expressing cells in the zebra finch brain. Developmental Neuroscience. 1999

Jeong JK, Burrows K, Tremere LA, Pinaud R. Neurochemical organization and experience-dependent activation of estrogen-associated circuits in the songbird auditory forebrain. Eur J Neurosci. 2011; 34:283–91. [PubMed: 21707790]

Kawaguchi Y, Kubota Y. GABAergic cell subtypes and their synaptic connections in rat frontal cortex. Cereb Cortex. 1997a; 7:476–486. [PubMed: 9276173]

Kawaguchi Y, Kubota Y. GABAergic cell subtypes and their synaptic connections in rat frontal cortex. Cereb Cortex. 1997b; 7:476–86. [PubMed: 9276173]

Kirn JR, Fishman Y, Sasportas K, Alvarez-Buylla A, Nottebohm F. Fate of new neurons in adult canary high vocal center during the first 30 days after their formation. J Comp Neurol. 1999; 411:487–494. [PubMed: 10413781]

Li J, Zhou X, Huang L, Fu X, Liu J, Zhang X, Sun Y, Zuo M. Alteration of CaBP expression pattern in the nucleus magnocellularis following unilateral cochlear ablation in adult zebra finches. PLoS One. 2013; 8:1–11.

Long MA, Jutras MJ, Connors BW, Burwell RD. Electrical synapses coordinate activity in the suprachiasmatic nucleus. Nat Neurosci. 2005; 8:61–66. [PubMed: 15580271]

Maney DL. The incentive salience of courtship vocalizations: Hormone-mediated “wanting” in the auditory system. Hear Res. 2013; 305:19–30. [PubMed: 23665125]

Markram H, Toledo-Rodriguez M, Wang Y, Gupta A, Silberberg G, Wu C. Interneurons of the neocortical inhibitory system. Nat Rev Neurosci. 2004; 5:793–807. [PubMed: 15378039]

Medina FS, Hunt GR, Gray RD, Wild JM, Kubke MF. Perineuronal satellite neuroglia in the telencephalon of New Caledonian crows and other Passeriformes: evidence of satellite glial cells in the central nervous system of healthy birds? PeerJ. 2013; 1:e110. [PubMed: 23904989]

Mehos CJ, Nelson LH, Saldanha CJ, Saldanha CJ. A Quantification of the Injury-Induced Changes in Central Aromatase. Oestrogenic Milieu and Steroid Receptor Expression in the Zebra Finch Neuroendocrinology. 2016

Metzdorf R, Gahr M, Fusani L. Distribution of aromatase, estrogen receptor, and androgen receptor mrna in the forebrain of songbirds and nonsongbirds. J Comp Neurol. 1999; 407:115–129. [PubMed: 10213192]

Meyer AH, Katona I, Blatow M, Rozov A, Monyer H. In Vivo Labeling of Parvalbumin-Positive Interneurons and Analysis of Electrical Coupling in Identified Neurons. J Neurosci. 2002; 22

Moe Y, Tanaka T, Morishita M, Ohata R, Nakahara C, Kawashima T, Maekawa F, Sakata I, Sakai T, Tsukahara S. A comparative study of sex difference in calbindin neurons among mice, musk shrews, and Japanese quails. Neurosci Lett. 2016; 631:63–69. [PubMed: 27531632]

Mooney R. Neural mechanisms for learned birdsong. Learn Mem. 2009; 16:655–69. [PubMed: 19850665]

Mullen RJ, Buck CR, Smith AM. NeuN, a neuronal specific nuclear protein in vertebrates. Development. 1992; 116:201–211. [PubMed: 1483388]

Noctor SC, Flint AC, Weissman TA, Dammerman RS, Kriegstein AR. Neurons derived from radial glial cells establish radial units in neocortex. Nature. 2001; 409:714–720. [PubMed: 11217860]

Olkowicz S, Kocourek M, Lučan RK, Porteš M, Fitch WT, Herculano-Houzel S, Němec P. Birds have primate-like numbers of neurons in the forebrain. Proc Natl Acad Sci U S A. 2016; 113:7255–60. [PubMed: 27298365]

Ono S, Okanoya K, Seki Y. Hierarchical emergence of sequence sensitivity in the songbird auditory forebrain. J Comp Physiol A. 2016; 202:163–183.

Peterson RS, Lee DW, Fernando G, Schlinger BA. Radial glia express aromatase in the injured zebra finch brain. J Comp Neurol. 2004; 475:261–269. [PubMed: 15211466]

Peterson RS, Yarram L, Schlinger BA, Saldanha CJ. Aromatase is pre-synaptic and sexually dimorphic in the adult zebra finch brain. 2005:2089–2096.

Pinaud R, Fortes AF, Lovell P, Mello CV. Calbindin-positive neurons reveal a sexual dimorphism within the songbird analogue of the mammalian auditory cortex. J Neurobiol. 2006; 66:182–195. [PubMed: 16288476]

Pinaud R, Mello CV. GABA immunoreactivity in auditory and song control brain areas of zebra finches. J Chem Neuroanat. 2007; 34:1–21. [PubMed: 17466487]

Pinet-Charvet C, Geller S, Desroziers E, Ottogalli M, Lomet D, Georgelin C, Tillet Y, Franceschini I, Vaudin P, Duittoz A. GnRH Episodic Secretion Is Altered by Pharmacological Blockade of Gap Junctions: Possible Involvement of Glial Cells. Endocrinology. 2016; 157:304–322. [PubMed: 26562259]

Remage-Healey L. Frank Beach Award Winner: Steroids as neuromodulators of brain circuits and behavior. Horm Behav. 2014; 66:552–560. [PubMed: 25110187]

Remage-Healey L, Coleman MJ, Oyama RK, Schlinger Ba. Brain estrogens rapidly strengthen auditory encoding and guide song preference in a songbird. Proc Natl Acad Sci U S A. 2010; 107:3852–3857. [PubMed: 20133597]

Remage-Healey L, Dong S, Maidment NT, Schlinger BA. Presynaptic Control of Rapid Estrogen Fluctuations in the Songbird Auditory Forebrain. J Neurosci. 2011; 31:10034–10038. [PubMed: 21734295]

Remage-Healey L, Joshi NR. Changing neuroestrogens within the auditory forebrain rapidly transform stimulus selectivity in a downstream sensorimotor nucleus. J Neurosci. 2012; 32:8231–8241. [PubMed: 22699904]

Remage-Healey L, Maidment NT, Schlinger BA. Forebrain steroid levels fluctuate rapidly during social interactions. Nat Neurosci. 2008; 11:1327–34. [PubMed: 18820691]

Remage-Healey L, Oyama RK, Schlinger BA. Elevated aromatase activity in forebrain synaptic terminals during song. J Neuroendocrinol. 2009; 21:191–199. [PubMed: 19207827]

Rohmann KN, Schlinger BA, Saldanha CJ. Subcellular compartmentalization of aromatase is sexually dimorphic in the adult zebra finch brain. Dev Neurobiol. 2007; 67:1–9. [PubMed: 17443767]

Runyan CA, Schummers J, Van Wart A, Kuhlman SJ, Wilson NR, Huang ZJ, Sur M. Response Features of Parvalbumin-Expressing Interneurons Suggest Precise Roles for Subtypes of Inhibition in Visual Cortex. Neuron. 2010; 67:847–857. [PubMed: 20826315]

Saldanha CJ, Tuerk MJ, Kim YH, Fernandes AO, Arnold AP, Schlinger BA. Distribution and regulation of telencephalic aromatase expression in the zebra finch revealed with a specific antibody. J Comp Neurol. 2000; 423:619–30. [PubMed: 10880992]

Schneider DM, Woolley SMN. Sparse and background-invariant coding of vocalizations in auditory scenes. Neuron. 2013; 79:141–52. [PubMed: 23849201]

Shen P, Schlinger BA, Campagnoni AT, Arnold AP. An atlas of aromatase mRNA expression in the zebra finch brain. J Comp Neurol. 1995; 360:172–184. [PubMed: 7499563]

Srivastava DP, Woolfrey KM, Penzes P. Insights into rapid modulation of neuroplasticity by brain estrogens. Pharmacol Rev. 2013; 65:1318–50. [PubMed: 24076546]

Venance L, Rozov A, Blatow M, Burnashev N, Feldmeyer D, Monyer H. Connexin expression in electrically coupled postnatal rat brain neurons. Proc Natl Acad Sci U S A. 2000; 97:10260–5. [PubMed: 10944183]

Vockel A, Pröve E, Balthazart J. Sex- and age-related differences in the activity of testosterone-metabolizing enzymes in microdissected nuclei of the zebra finch brain. 1990

Werker JF, Hensch TK. Critical Periods in Speech Perception: New Directions. Annu Rev Psychol. 2015; 66:173–196. [PubMed: 25251488]

Wild JM, Williams MN, Howie GJ, Mooney R. Calcium-binding proteins define interneurons in HVC of the zebra finch (Taeniopygia guttata). J Comp Neurol. 2005; 483:76–90. [PubMed: 15672397]

Yague JG, Wang AC-J, Janssen WGM, Hof PR, Garcia-Segura LM, Azcoitia I, Morrison JH. Aromatase distribution in the monkey temporal neocortex and hippocampus. Brain Res. 2008; 1209:115–127. [PubMed: 18402929]

Yague JGG, Muñoz A, de Monasterio-Schrader P, DeFelipe J, Garcia-Segura LM, Azcoitia I. Aromatase expression in the human temporal cortex. Neuroscience. 2006; 138:389–401. [PubMed: 16426763]

Yanagihara S, Yazaki-Sugiyama Y. Auditory experience-dependent cortical circuit shaping for memory formation in bird song learning. Nat Commun. 2016; 7:11946. [PubMed: 27327620]

Yang QZ, Hatton GI. Direct evidence for electrical coupling among rat supraoptic nucleus neurons. 1988

Zimmerman ME, Lipton RB, Santoro N, McConnell DS, Derby CA, Katz MJ, Baigi K, Saunders-Pullman R. Endogenous estradiol is associated with verbal memory in nondemented older men. Brain Cogn. 2011; 76:158–165. [PubMed: 21354686]

Table of Abbreviations

HP	hippocampus
NCL	caudolateral nidopallium
NCMv	caudomedial nidopallium ventral
NCMd	caudomedial nidopallium dorsal
RA	robust nucleus of arcopallium
CMM	caudal medial mesopallium
PSD-95	postsynaptic density-95

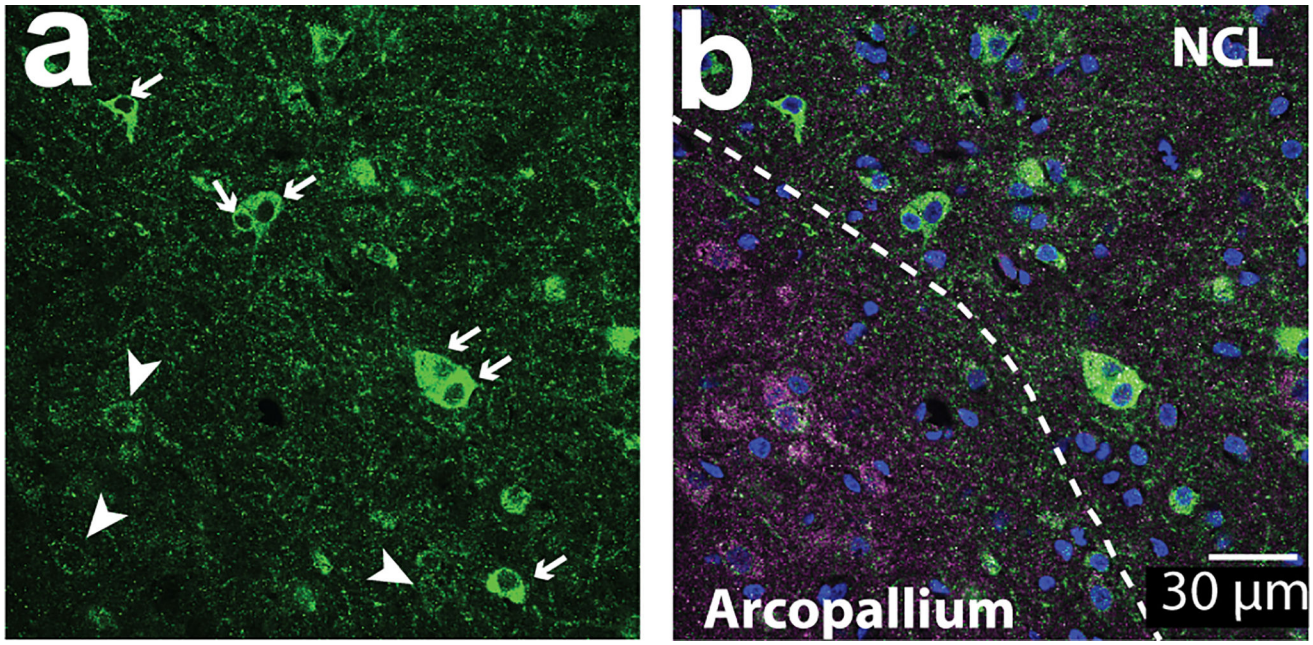

Figure 1. Aromatase+ cells included in analysis along with excluded "ghost cells"

60× single z-image at the border between arcopallium and NCL from tissue stained against PSD-95 (magenta), aromatase (green), and DAPI (blue). **(a)** High-intensity fluorescent cells (arrows, "aromatase+ cells") are located in the NCL, while low-intensity fluorescent cells (arrow heads, "ghost cells") are shown here in the same section image overlapping with PSD-95 signals **(b)** and located primarily in the arcopallium. Ghost cells are likely to reflect inputs consisting of pre-synaptic aromatase-positive terminals, as described by (Saldanha et al., 2000).

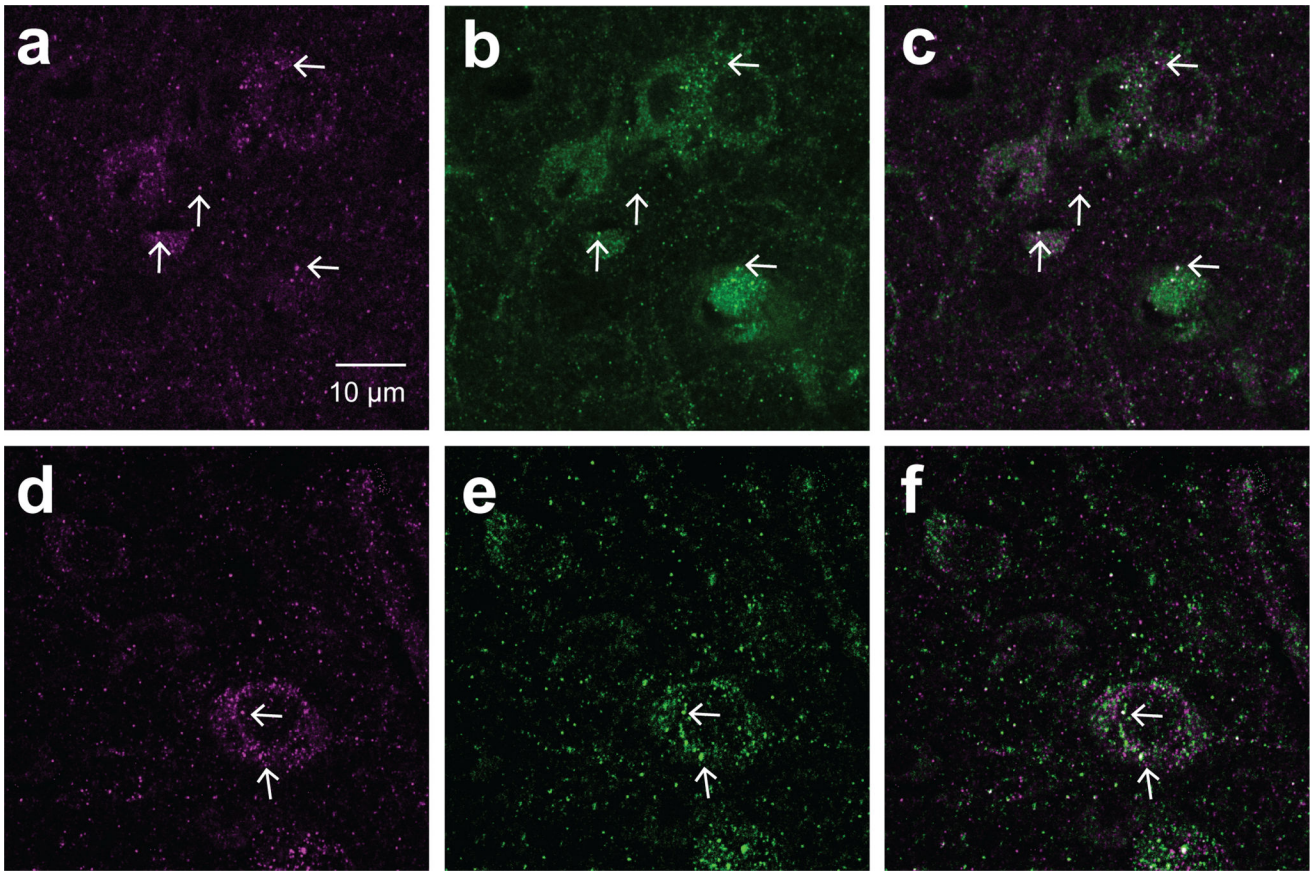

Figure 2. PSD-95 and aromatase puncta are localized in close proximity

Sections were stained with antibodies specific for aromatase (green) and PSD-95 (magenta) in NCL **(a–c)** and the arcopallium **(d–f)** were imaged with a confocal microscope. The *white arrows* show co-localizing puncta as supporting evidence for pre-synaptic aromatase+ terminals forming synapses.

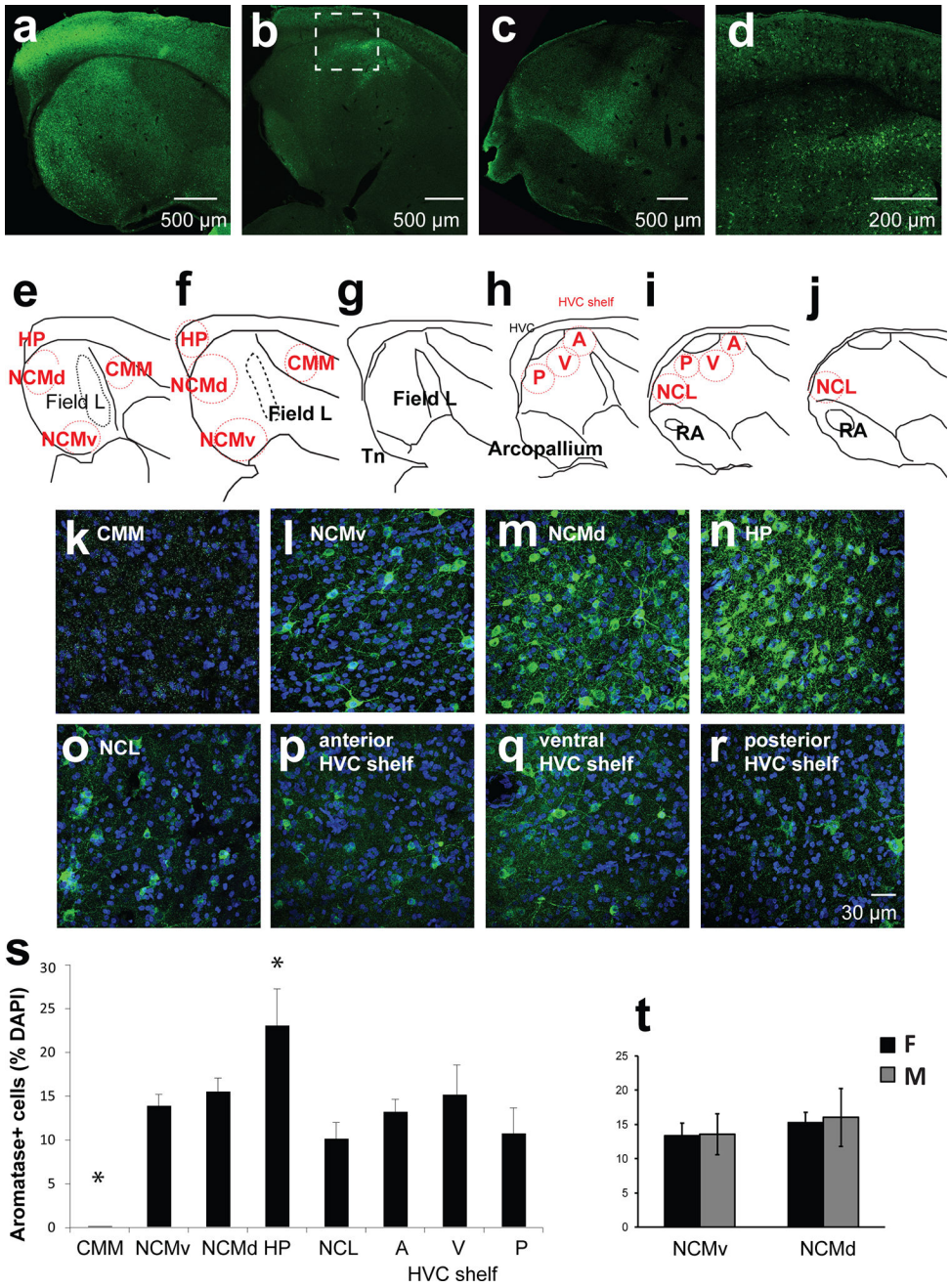

Figure 3. Regions of interest and cellular aromatase expression patterns

Female and male zebra finch brains were stained with aromatase antibody (green) and DAPI (blue) and imaged using a confocal microscope. **(a–d)** 10× stitch images of example sagittal sections to demonstrate the anatomy of regions of interest. Dotted box indicates where HVC and HVC shelf are located. **(e–j)** Illustrations of sagittal sections medial (left) to lateral (right) (~0.5 – 2.2 mm from midline, ~0.3 mm apart). Red circles are approximate areas where 60× images were taken for counting aromatase+ cells. These circles do not represent actual size of images respective to sections. A-anterior; V-ventral; P-posterior; D-Dorsal. Modified illustrations from ZEBrA: A Zebra Finch Expression Atlas, RRID: nif-0000–

24345; http://www.zebrafinchatlas.org. (**k–q**) Maximum-intensity projection images from regions of interest using a 60× objective. (**s**) Percentage of aromatase-expressing cells among DAPI+ cells in each region of interest. HP and CMM are significantly different from other regions (Mean ± SEM*, $p < 0.05$). CMM, N= 10; NCMv, N= 11; NCMd, N= 11; HP, N= 11; NCL, N= 8; HVCshelf: A, N=8; V, N=8; P, N=8. **(t)** Percentage of aromatase-expressing cells among DAPI+ cells in females (F, n=6) and males (M, n=5) for NCMv and NCMd.

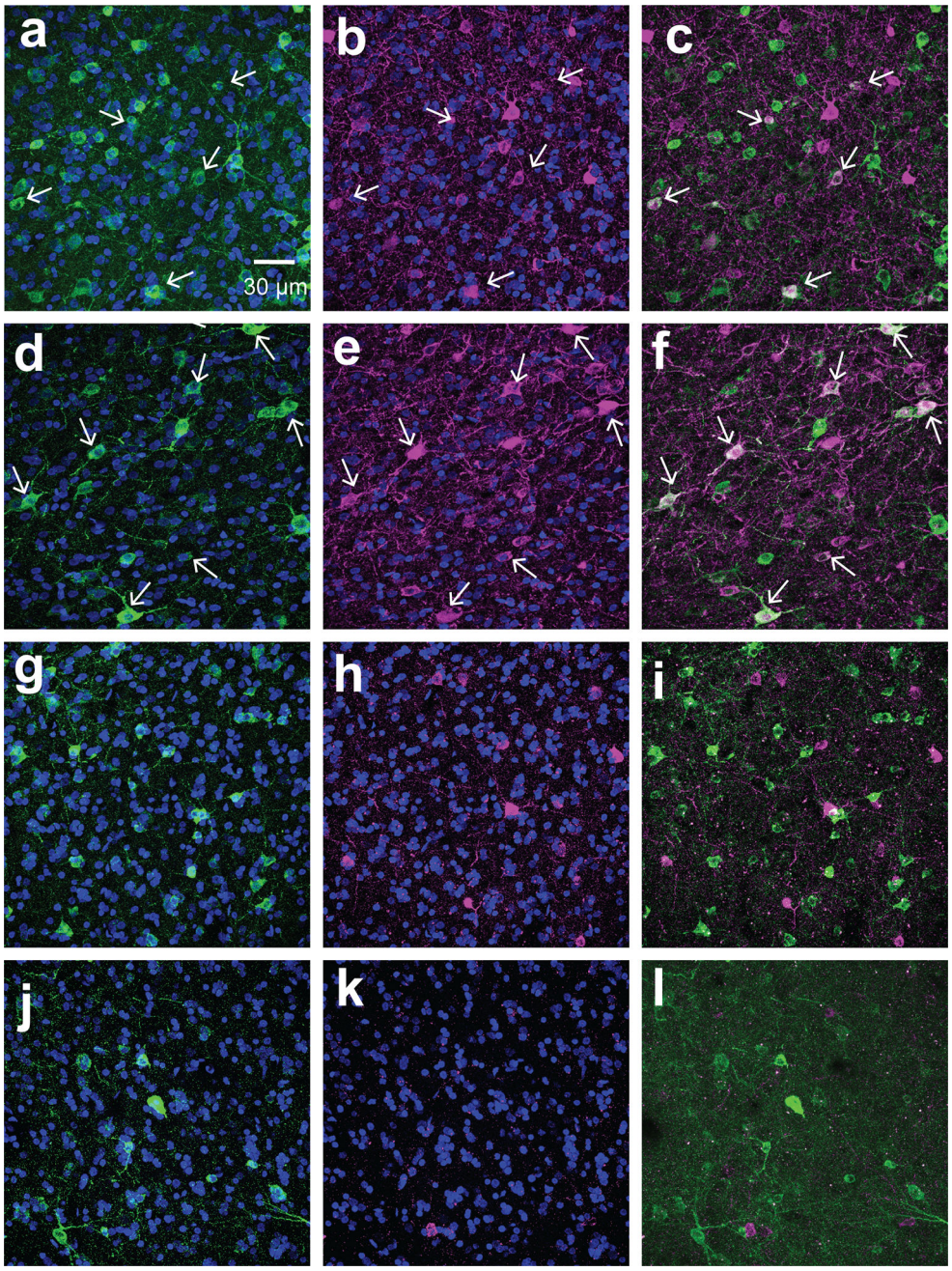

Figure 4. Aromatase coexpresses with PV but not CB

Examples of 60× maximum intensity projection images from medial NCM (dorsal: **a–c, g–i**; ventral: **d–f, j–l**) sections double-labeled either for aromatase (green) and PV (magenta; **a–f**) or aromatase and CB (magenta; **g–l**) from a subject with high co-expression of PV and aromatase. *White arrows* indicate cells coexpressing aromatase and PV.

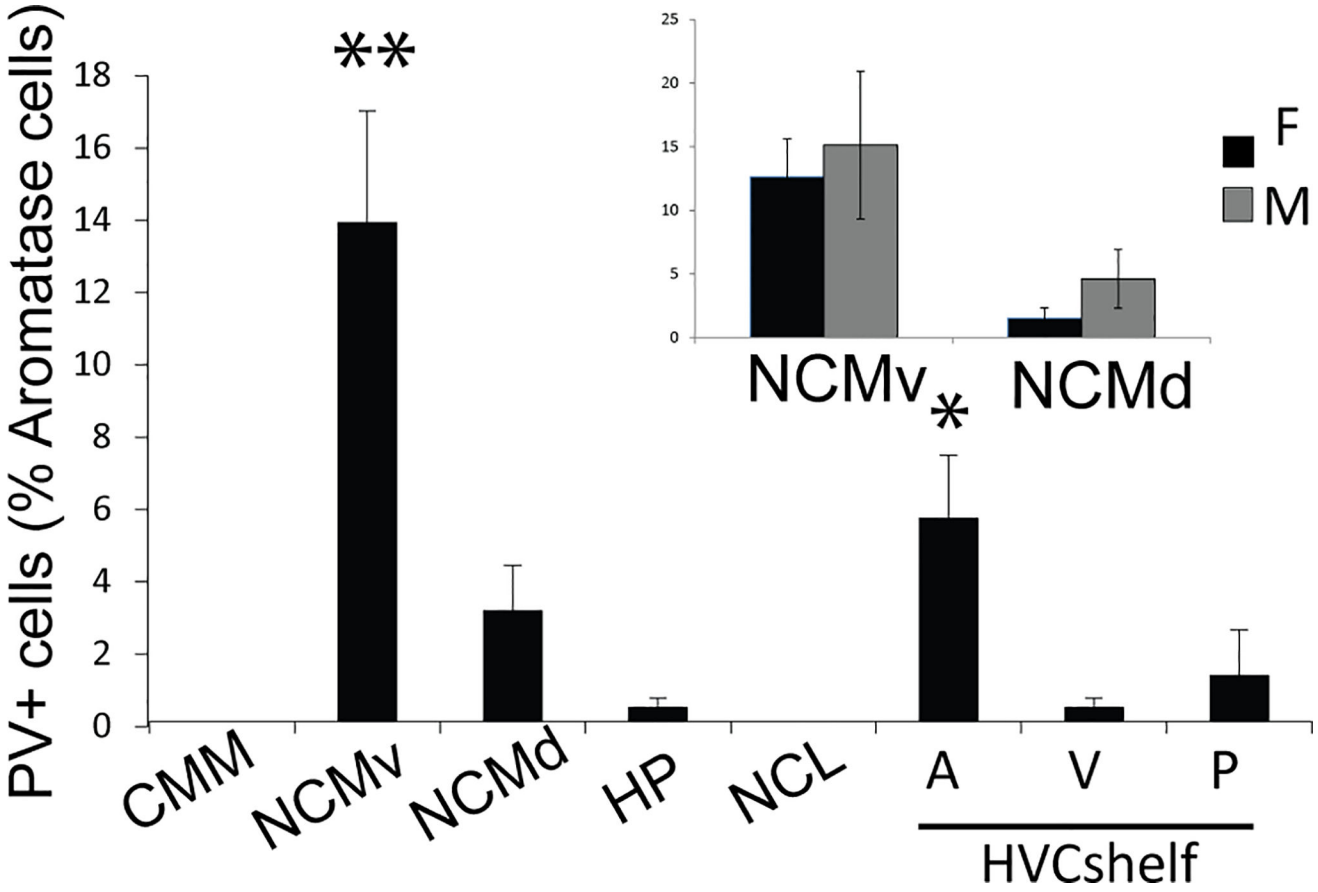

Figure 5. A subset of aromatase+ cells co-express PV

Quantification of PV+ aromatase+ cells. Inset, data from NCM separated by sex. No significant differences are found between the two sexes (Anova, Sex*Region: $p>0.05$; Sex, $p>0.05$; Region, $p=0.038$). CMM, N=9; NCMv, N=11; NCMd, N=11; HP, N=9; NCL, N=7; HVCshelf: A, N=8; V, N=8; P, N=8. Asterisks indicate significant regional differences. $p<.05$*, $p<.01$**.

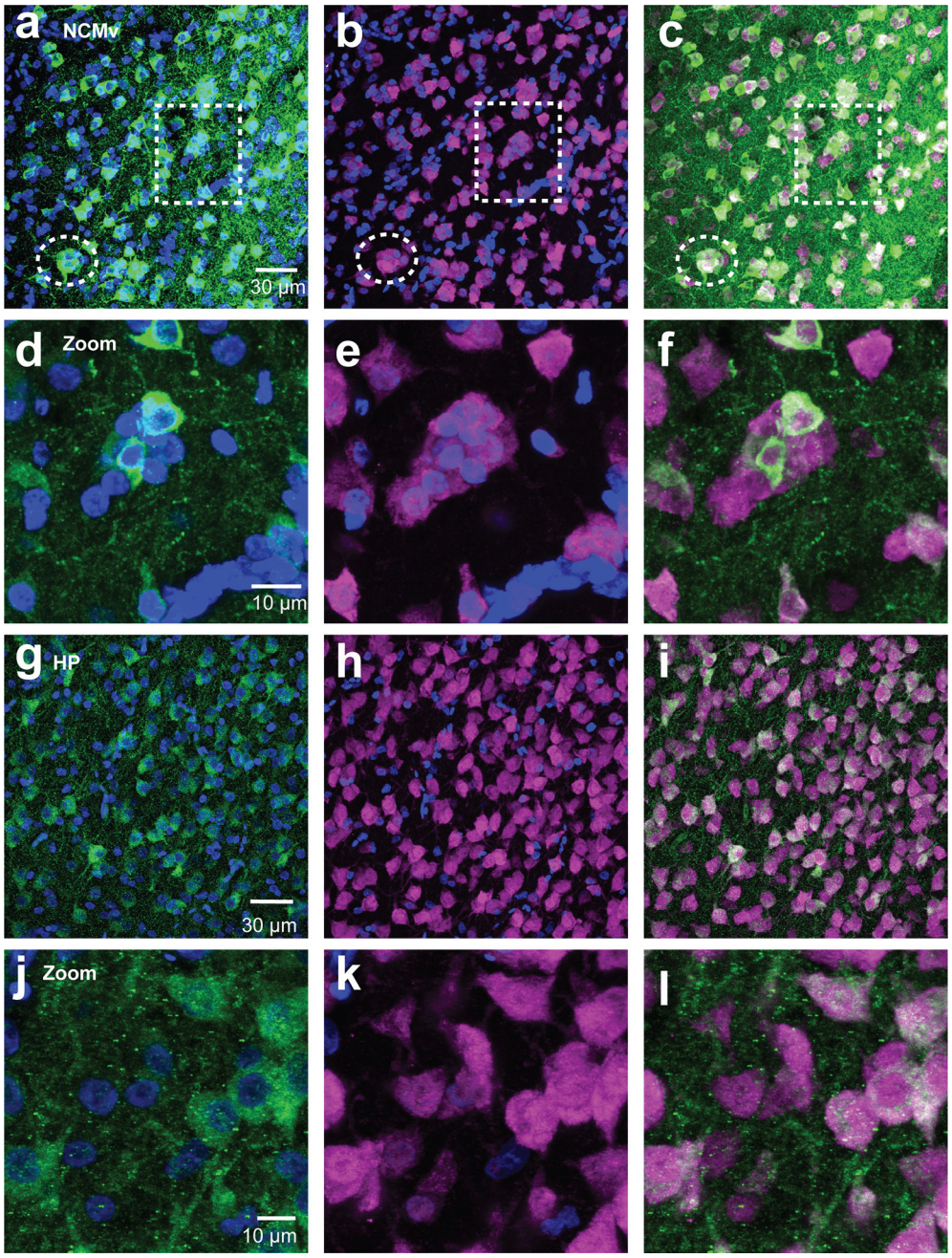

Figure 6. Aromatase cells are found in neuronal clusters of NCM and not HP

Maximum intensity projection images of 60× z-stack images taken from NeuN (magenta) and aromatase (green) double-labeled sections of NCMv **(a–f)** and HP **(g–l)**. Exemplars of NeuN clusters in NCMv are noted with dotted lines **(a–c)**. Images in the second row of each region (NCMv: **d–f**, HP: **j–l**) are zoomed-in images of the cluster in the dotted square in the first row for NCMv and illustrating the lack of compact clustering for HP.

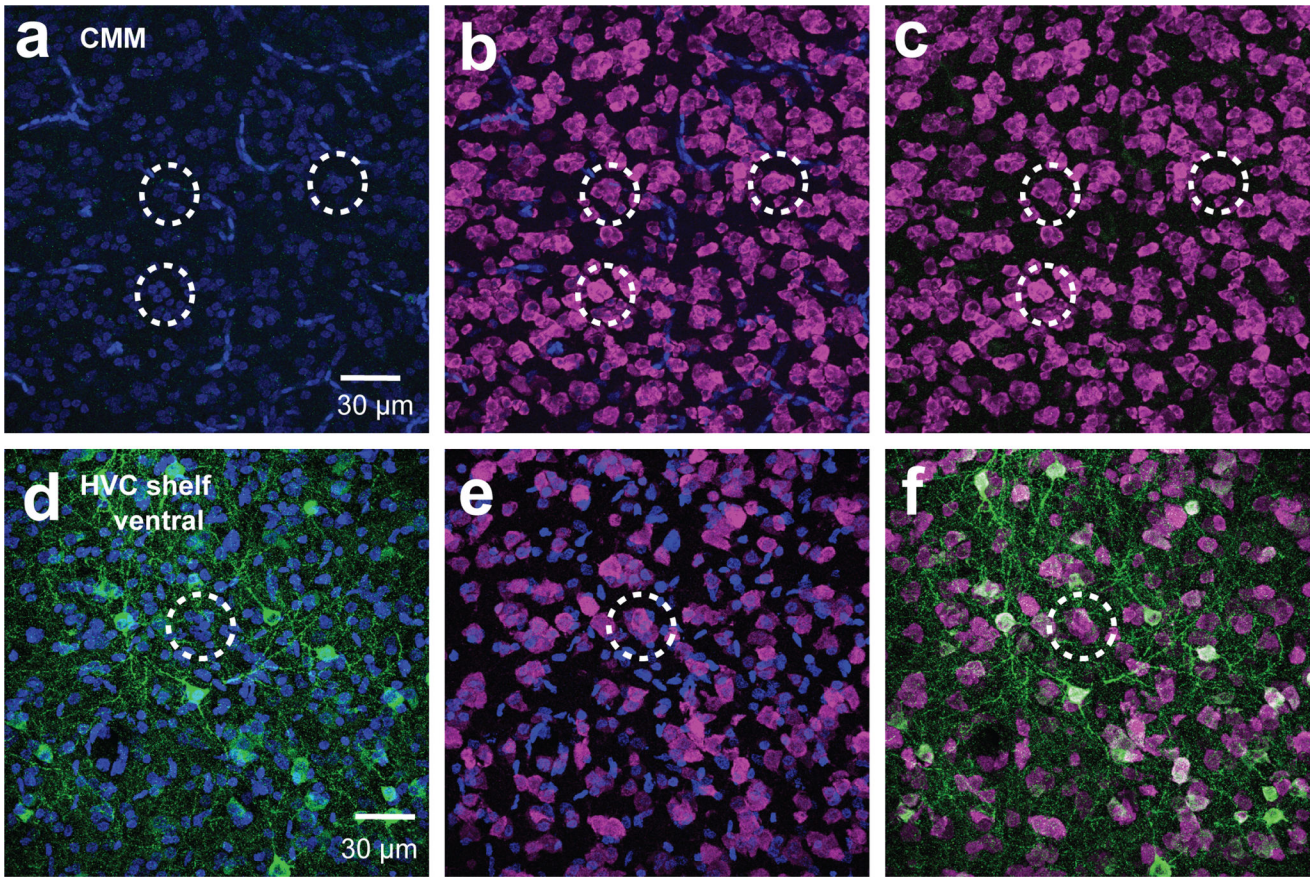

Figure 7. Aromatase- cells are also found in neuronal clusters in CMM and HVCshelf

Maximum intensity projection images of 60× z-stack images taken from NeuN (magenta) and aromatase (green) double-labeled sections. CMM **(a–c)** which lacks aromatase and HVC shelf ventral **(d–f)** which contains aromatase also contain neuronal clusters that do not have aromatase expressing cells (unquantified).

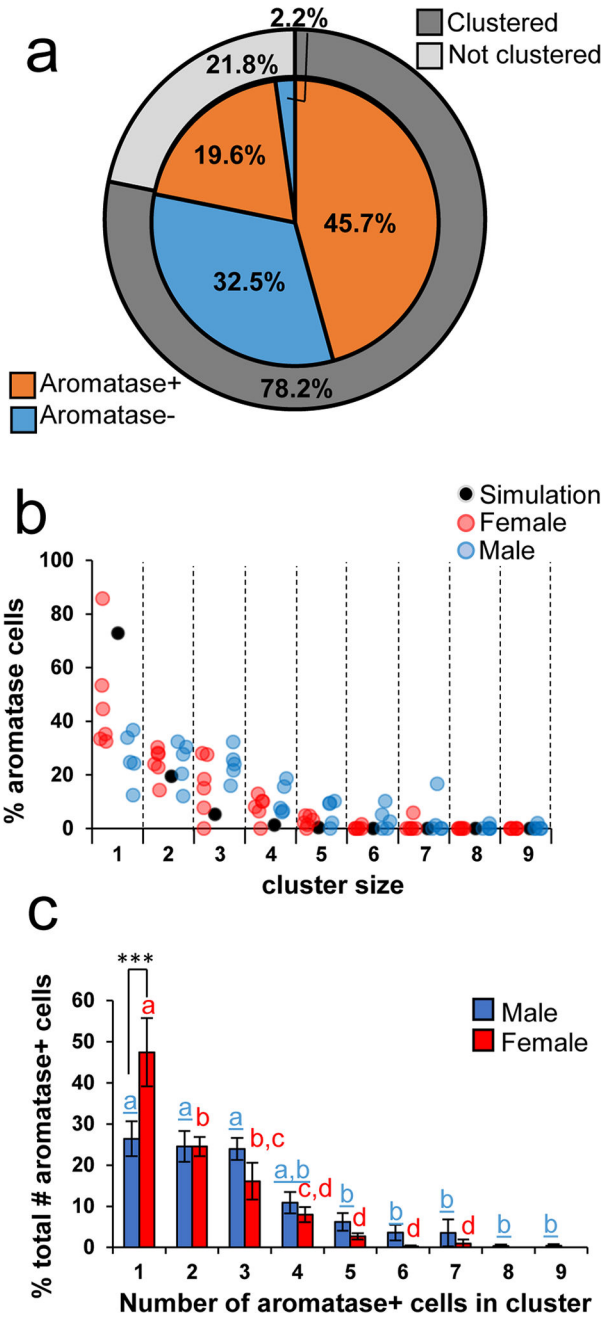

Figure 8. The majority of aromatase+ cells are neurons and are found in dense clusters

(**a**), Percentages of clustered, not clustered, aromatase+, and aromatase- neurons in the image from NCMv in Figure 6a–c. **(b)** Percentages of aromatase cells for each male and female subjects with increasing cluster sizes. Red dots are female subjects and blue dots are male subjects. Black dots indicate the average number of cells found in cluster sizes across 1000 simulations to indicate the population average of the simulation. **(c)**, Percentages of aromatase+ cells found in clusters with increasing numbers of other aromatase+ cells (N=11, Males (blue) N=5, Females (red) N=6). Females have a higher proportion of aromatase cells found not clustered (1; p<.001***). As cluster sizes increase, females have a precipitous

decline in the distribution. Males have similar proportions of aromatase cells found in cluster sizes up to 4, and then these proportions decline for cluster categories greater than 5. Significant sex differences grouped by cluster sizes are represented by asterisks (*) and regional Bonferroni post-hoc comparisons are represented by letters and columns with a different letter are significantly different. Male letters are blue and underlined and female letters are red.

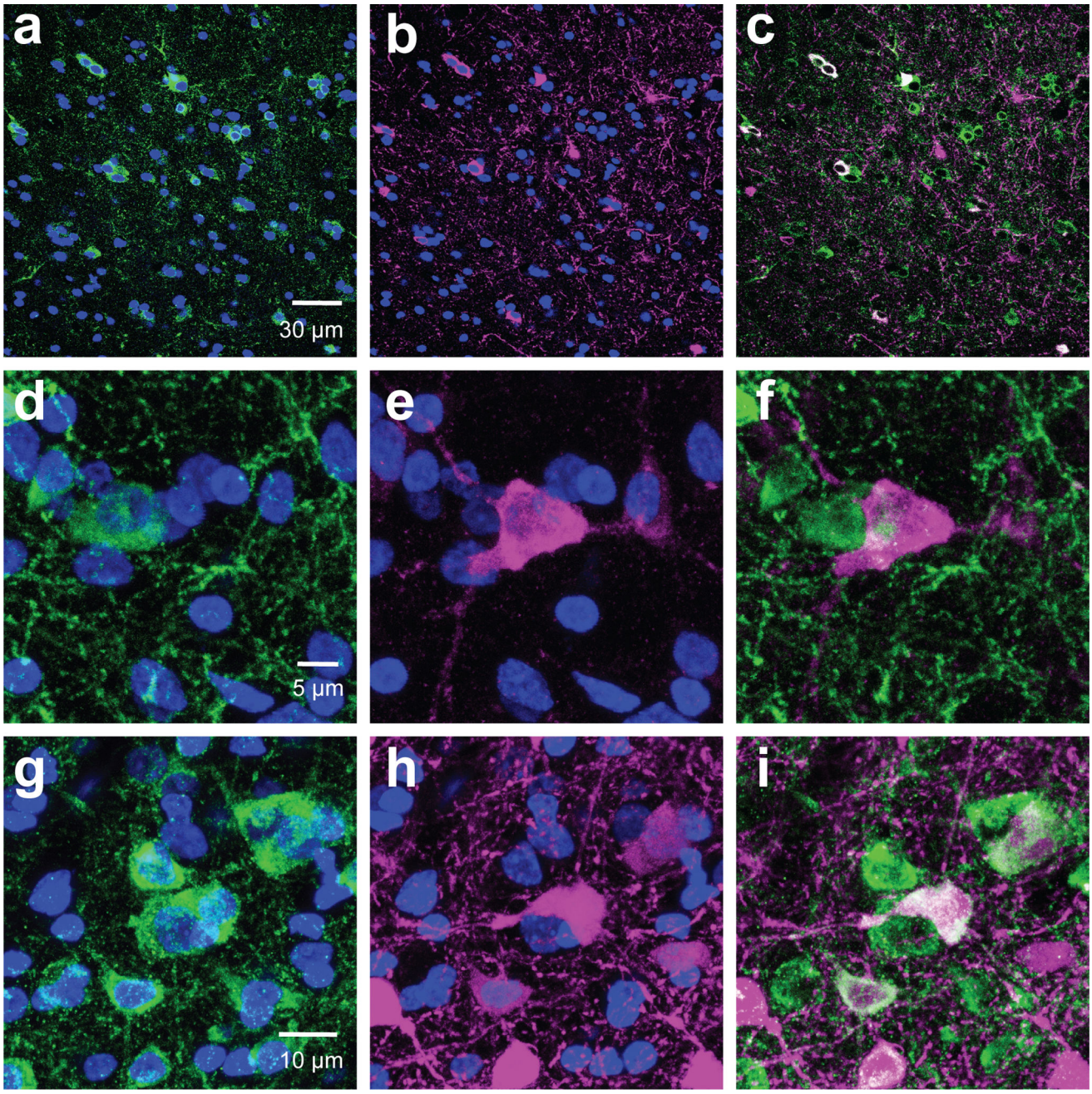

Figure 9. Aromatase cells are clustered with PV cells

Examples of **(a–i)** aromatase+ cell bodies (green) clustered with PV+ (magenta). **a–c** are single 60× z-images in NCMv. **d–i**, Maximum intensity projection of zoomed-in 60× z-stack images of exemplars of aromatase clusters with PV+Aromatase- cells **(d–f)**, PV+Aromatase + cells **(g–i)**..

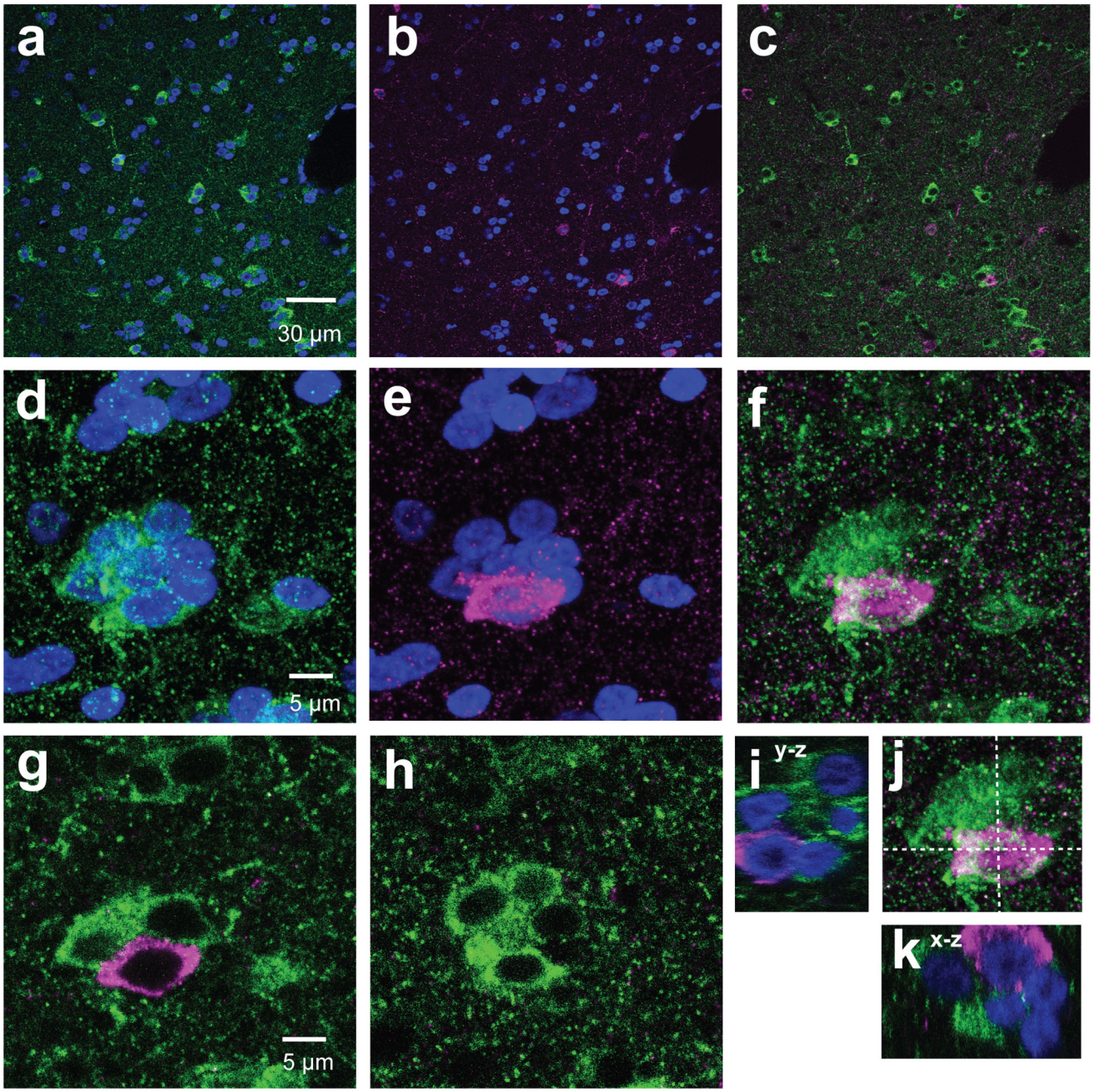

Figure 10. Aromatase cells are clustered with CB cells

Examples of **(a–f)** aromatase+ cell bodies (green) clustered with CB+ (magenta). **a–c** are single 60× z-images in NCMv. **d–k**, Maximum intensity projection of zoomed-in 60× z-stack images of exemplars of aromatase clusters with CB+Aromatase- cells. **g & h** are two single z-images from cluster shown in **f** to illustrate that the CB+ cell (magenta) in **f** is not co-expressing aromatase (green). **i–k** are orthogonal depth-profile images (y–z and x–z images) of the maximum intensity projection image in **f**.

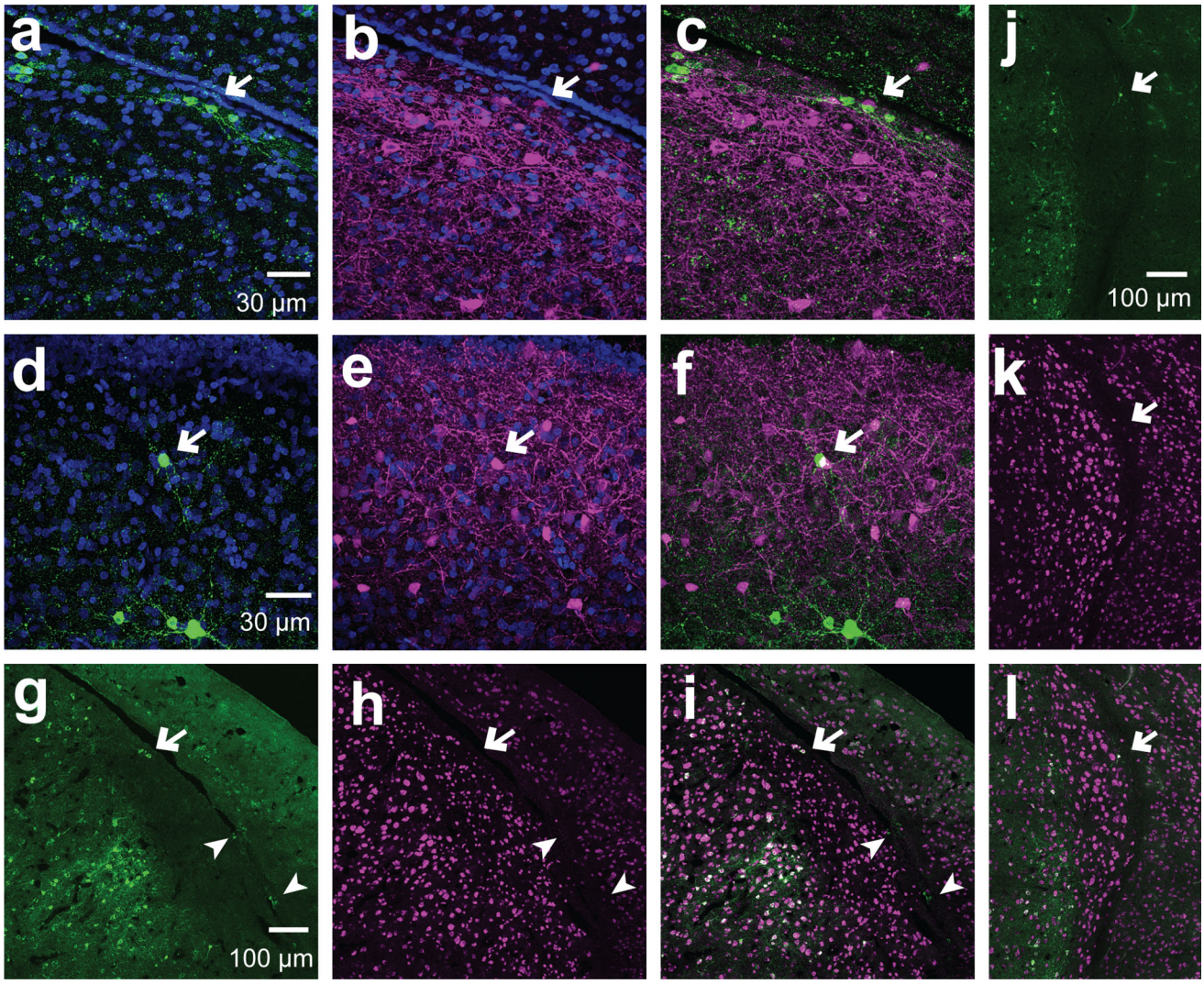

Figure 11. Aromatase cells are positive and negative for NeuN in the HVC

Exemplars of aromatase+ neurons in the HVC. (**a–f**) Maximum intensity projections of 60× z-stack stitch images of sagittal sections stained for aromatase (green) and PV (magenta). **a–c**, aromatase+ cells close to the ventricle. **d–f**, aromatase+ cell in the middle of the HVC away from the HVC shelf and ventricle. (**g–l** Maximum intensity projections of 60× stitched z-stack images of sagittal sections stained for aromatase (green) and NeuN (magenta). Aromatase+ cells in the HVC away from the ventricle are NeuN+ (arrows), while aromatase + cells at the edge of the tissue are negative for NeuN (arrow heads).

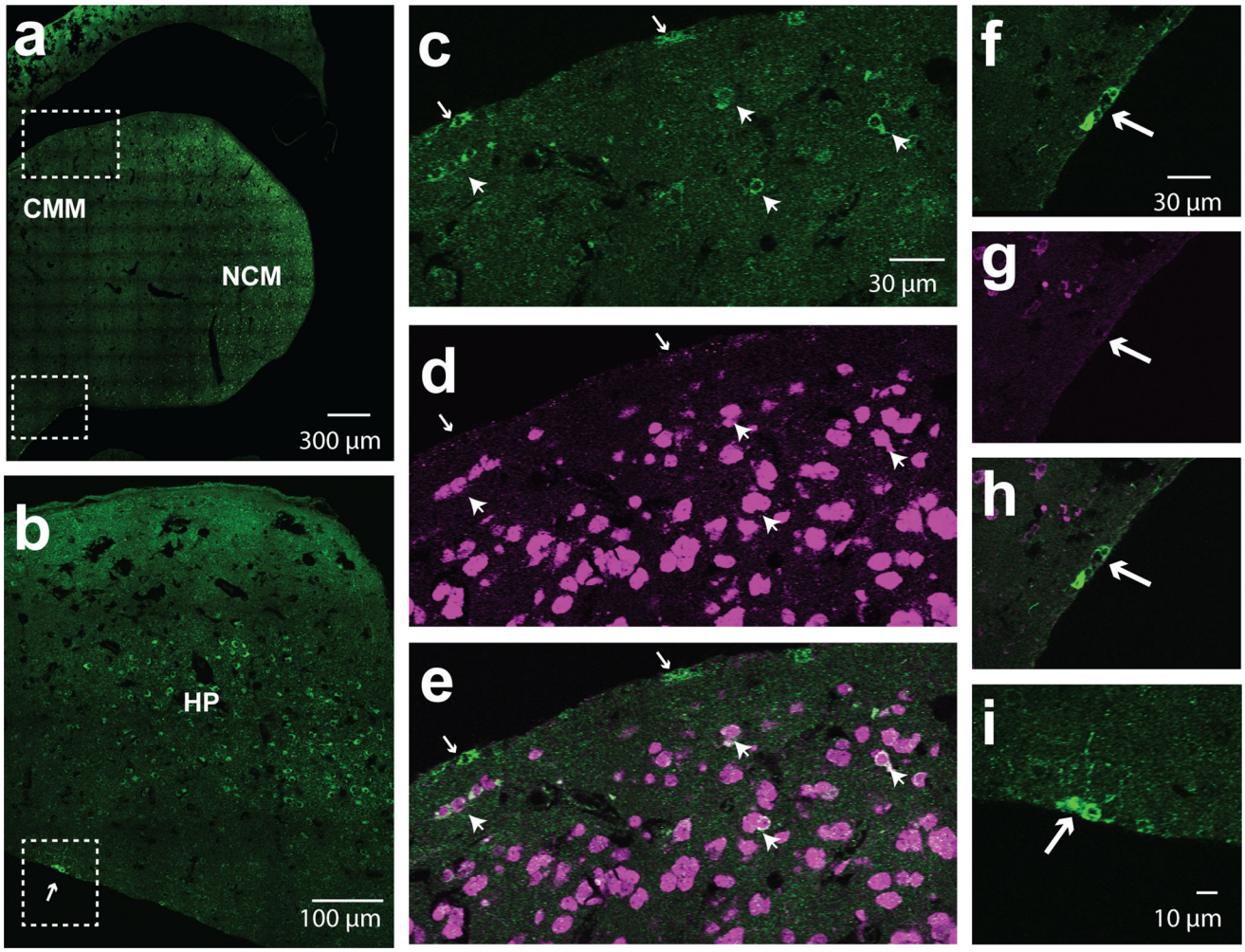

Figure 12. Aromatase+ cells in the CMM and HP

(**a**) 60× stitched single z-image of a sagittal section from the caudal medial telencephalon (CMM) stained for aromatase (green) and NeuN (magenta; only the fluorescent signal for aromatase is shown). **(b)** 60× single z-image of a hippocampus sectioned in the sagittal plane stained for aromatase.(**c–e**) Cropped, zoomed-in images of area surrounded by white dashed lines in dorsal CMM in **a**. *White arrows* show examples of aromatase+ cells that are negative for NeuN at the edge of the tissue. *White arrow heads* point to aromatase+ neurons positive for NeuN. **(f–g)** Cropped, zoomed-in images of area surrounded by white dashed lines in ventralnidopallium. *White arrows* show examples of aromatase+ cells that are negative for NeuN at the edge of the tissue. *White arrow heads* point to aromatase+ neurons positive for NeuN. **(h–i)**, Zoom-in image of dotted-square in **b**. *White arrow* indicates neurons aligning the lateral ventricle.

Table 1

Antibodies used in this study

Antibody	Source	Manufacturer	Dilution
anti-aromatase	Synthetic peptide residues “RRNANENQGDGMDQH” corresponding to predicted a.a. sequences 495–509 at the 3’ terminal of zebra finch aromatase (Saldanha et al., 2000)	gift from Dr. Saldanha rabbit, polyclonal	1:2000
anti-calbindin	Raised against bovine kidney calbindin-D	Sigma Aldrich, C9848 RRID: AB_476894 mouse, monoclonal (CB-955)	1:2000
anti-parvalbumin	Parvalbumin purified from frog muscle	Millipore, MAB1572, RRID: AB_2174013 mouse, monoclonal (PARV-19)	1:10,000
anti-PSD95	Recombinant rat PSD-95	Millipore, MAB1596, RRID: AB_2092365 mouse, monoclonal (clone 6G6-1C9)	1:1000
anti-NeuN	Purified cell nuclei from mouse brain	Millipore, MAB377 RRID: AB_2298772 mouse, monoclonal (clone A60)	1:2000–1:5000

Abbreviations: PSD, post-synaptic density; NeuN, neuronal nuclei

Table 2

Sex differences in aromatase cluster size

	Cluster size									
	1	**2**	**3**	**4**	**5**	**6**	**7**	**8**	**9**	**Sex**
Avg # of clusters found	NA	13.2	8.60	3.77	1.67	1.07	0.87	0.10	0.10	*male*
	NA	9.19	4.30	1.67	0.49	0.042	0.084	0	0	*female*
# of subjects with that cluster size	5	5	5	5	4	3	2	1	1	*male*
	6	6	5	5	5	1	1	0	0	*female*

Abbreviations: Avg, average; NA, not applicable; #, number